Proceedings of the
Annual Stability Conference
Structural Stability Research Council
Louisville, Kentucky, April 1-4, 2025

Practical stability design of general I-section members for combined forces

Donald W. White[1], Bálint Vaszilievits-Sömjén[2]

Abstract
Numerous situations occur in engineering practice where I-section members must be designed for a combination of flexure, shear, torsion, and/or axial loadings. Particularly in metal buildings and horizontally curved I-girder bridges, these member types may have variable web depth and stepped cross-section transitions along their length. Design guidance for handling combined loadings on these member types has been limited. Modern software systems that can accurately calculate combined second-order elastic demands and elastic buckling loads for general I-section members in general framing systems are increasingly available. This paper discusses new AISC 360 Chapter F provisions under consideration in the 2027 Specification development cycle. These provisions provide an improved, streamlined calculation of the flexural resistance of general I-section members. The calculations address recent research findings regarding the influence of moment gradient and corresponding web shear. The discussion of the new AISC 360 procedures is followed by a brief presentation of recommended ways to verify a design where the member is also subjected to axial compression and/or torsion based on experiences from European and American practice. The focus of the paper is on the essential concepts.

1. Introduction
In recent years, many exciting developments have occurred in the AISC 360 and AASHTO LRFD Specifications and the Eurocode 3 Standard. The I-section member provisions in the AISC 360 Specification (AISC 2022) have been the subject of intensive research and committee evaluation during the 2022 and 2027 Specification cycles. The AASHTO LRFD 9th and 10th Edition Specifications (AASHTO 2020 and 2024) have incorporated substantial developments addressing nonprismatic girder design and the design verification of bridge members for general flexure, shear, torsion, and/or axial loadings. In European practice, substantial developments have occurred in practical analysis-design software systems allowing for accurate geometric nonlinear analysis of I-section members and frames for general loadings using frame elements based on thin-walled open-section beam theory (ConSteel 2025). These software systems also support the design of nonprismatic members using the so-called General Method (CEN 2022; Vaszilievits-Sömjén et al. 2023).

[1] Professor, Civil and Environmental Engineering, Georgia Institute of Technology, <dwhite@ce.gatech.edu>
[2] Senior Research Engineer, Consteel Solutions Ltd, Hungary <balint.vaszilievits@consteelsoftware.com>, PhD Student, Széchenyi István Egyetem, Győr, Hungary

Section 2 of this paper discusses the recent AISC 360 Chapter F developments. Section 3 elaborates on how the flexural resistance verifications in AISC 360 Chapter F can be extended most effectively to address combined axial compression and flexure in general I-section members. Section 4 then discusses combined flexure and torsion design with or without significant axial compression.

2. AISC 360-27 Chapter F Developments

Section F3 in the draft AISC 360-27 Standard under consideration by the AISC Specification Committee has consolidated the knowledge from the prior AISC 360 Sections F3 through F5 and substantive results from recent research into a single set of unified and streamlined procedures for the flexural design of general I-section members. The new Section F3 provisions are subdivided into three main subsections characterizing the following limit states: (1) Yielding and web local buckling (WLB), (2) Flange local buckling (FLB) and its potential interaction with yielding and WLB, and (3) Lateral-torsional buckling (LTB) and its potential interaction with yielding and WLB. The essential concepts and procedures employed to characterize these limit states are described in the following.

2.1 Yielding and web local buckling (WLB)

The draft AISC 360-27 Section F3 provisions define a “plateau” (i.e., maximum) strength for the FLB and LTB resistances by considering flexural yielding and its interaction with WLB. In many respects, the flexural yielding and WLB provisions are equivalent to the AISC 360-22 Section F4 and F5 provisions involving the web plastification factors, R_{pc} and R_{pt}, and the web bend buckling strength reduction factor, R_{pg}; however, the new provisions are more direct:

(a) For a compact web ($\lambda_w \leq \lambda_{pw}$)

$$M_w = M_p \tag{1a}$$

(b) For a noncompact web ($\lambda_{pw} < \lambda_w \leq \lambda_{rw}$)

$$M_w = M_p - \left(M_p - M_{yc}\right)\left(\frac{\lambda_w - \lambda_{pw}}{\lambda_{rw} - \lambda_{pw}}\right) \tag{1b}$$

and (c) For a slender web ($\lambda_w > \lambda_{rw}$)

$$M_w = R_b M_{yc} \tag{1c}$$

where M_w is the plateau resistance, M_p is the traditional cross-section plastic moment, M_{yc} is the moment at the nominal first yielding of the compression flange, λ_w is the web slenderness defined as h_{cy} / t_w in which h_{cy} is two times the depth of the web in flexural compression at the first yield of the compression flange and t_w is the web thickness, λ_{pw} and λ_{rw} are the compact- and noncompact-web limits associated with λ_w, and R_b is the web elastic bend buckling strength reduction factor written in terms of λ_w. Figure 1 shows a representative variation of the "plateau" strength associated with yielding and WLB as a function of the web slenderness λ_w.

For doubly-symmetric sections and singly-symmetric sections with the smaller flange in compression (such that the elastic section modulus to the tension flange is greater than or equal to the elastic section modulus to the compression flange, $S_{xt} \geq S_{xc}$), M_{yc} and h_{cy} are the traditional yield moment to the compression flange, $F_y S_{xc}$, and two times the elastic depth of the web in compression, h_c. However, for sections with a larger flange in compression such that $S_{xt} < S_{xc}$, the nominal first yielding occurs in tension and M_{yc} is the moment corresponding to a stress distribution such as that illustrated in Fig. 2. The Commentary of the draft Specification provides closed-form equations for the calculation of M_{yc} and h_{cy} for sections with these characteristics.

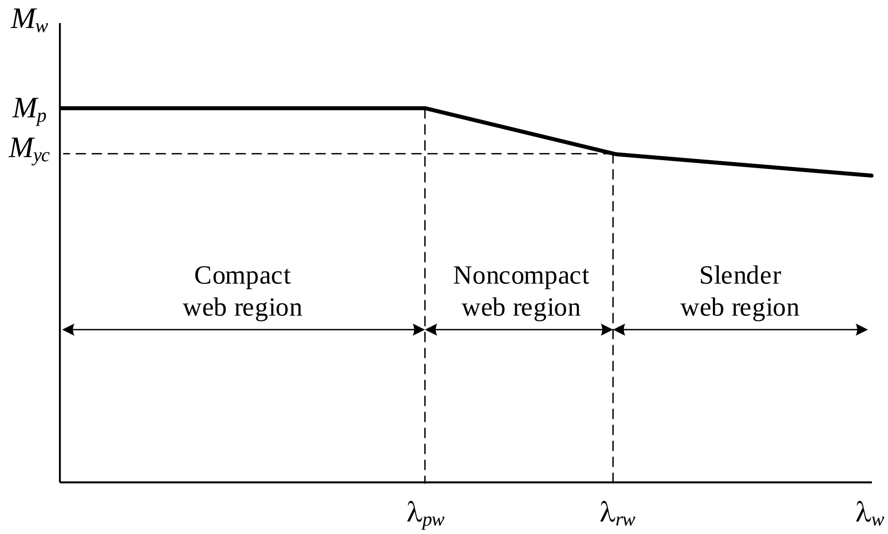

Figure 1: Representative variation in the "plateau" strength versus the web slenderness λ_w

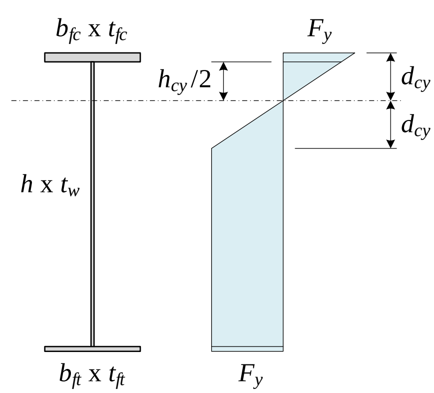

Figure 2: Representative stress distribution corresponding to M_{yc} for a section that yields first in tension

Defining M_{yc} as the "true" moment at the nominal first yielding of the compression flange and h_{cy} as two times the depth of the web in compression at this moment level addresses the fundamental mechanics of the flexural behavior directly and accurately, removing any need for the AISC 360-22 Tension Flange Yielding resistance calculations. In addition, the compact-web limit is defined using the general form given by Case 16 of the AISC 360-22 Table B4.1b, with h_{cy} substituted for h_c and M_{yc} for M_y,

$$\lambda_{pw} = \frac{\dfrac{h_{cy}}{h_p}\sqrt{\dfrac{E}{F_y}}}{\left(0.54\dfrac{M_p}{M_{yc}} - 0.09\right)^2} \tag{2}$$

In Eq. 2, h_p is two times the fully plastic depth of the web in compression. For a doubly-symmetric welded section, $h_{cy} = h_c = h_p = h$, where h_c is two times the elastic depth of the web in compression and h is the web depth between the insides of the flanges. Furthermore, the noncompact web limit is defined in the draft AISC 360-27 Specification as

$$\lambda_{rw} = c_{rw}\sqrt{\frac{E}{F_y}} \tag{3}$$

where c_{rw} varies between 4.6 and 5.7 as a function of $a_w = h_{cy}\, t_w \,/\, b_{fc}\, t_{fc}$. The above equations provide an improved characterization of the compact- and noncompact-web limits, recognizing that cross-sections where the neutral axis is close to the compression flange (and thus the web is loaded predominantly in flexural tension) can often develop the plastic moment (Slein et al. 2024) and recognizing the sensitivity of the noncompact-web limit to a_w (Subramanian and White 2017).

Lastly, the bend buckling strength reduction factor, R_b, is similar to the factor R_{pg} in AISC 360-22 but using the above definitions of a_w, λ_w, and λ_{rw}:

$$R_b = 1 - \frac{a_w}{1200 + 300a_w}\left(\lambda_w - \lambda_{rw}\right) \le 1.0 \tag{4}$$

2.2 Flange local buckling (FLB)

The draft AISC 360-27 Section F3 provisions define the FLB resistance by increasing the ordinate of the FLB strength curve at the AISC 360-22 noncompact flange limit, λ_{rf}, from $0.7F_y\, S_{xc}$ to $0.75F_y\, S_{xc}$ and extending the linear equation for the noncompact flange strength into the slender flange range (see Fig. 3), i.e.,

$$M_{n.FLB} = M_w - \left(M_w - 0.75R_b M_{yc}\right)\left(\frac{\lambda_f - \lambda_{pf}}{\lambda_{rf} - \lambda_{pf}}\right) \tag{5}$$

where $\lambda_f = b_{fc}/2t_{fc}$, λ_{pf} and λ_{rf} are the traditional AISC compact- and noncompact-flange slenderness limits, and M_w is the "plateau" strength defined by Eqs. 1. For $\lambda_f \le \lambda_{pf}$, the FLB resistance is equal to the "plateau" strength, M_w.

Equation 5 gives an accurate to conservative representation of the compression flange postbuckling strength in I-section members (Latif and White 2022). For extremely large λ_f values, Eq. 5 can potentially give a strength smaller than the theoretical elastic FLB resistance. This occurrence is disallowed in the Specification provisions; however, λ_f values this large are extremely rare. For instance, the AASHTO LRFD Specifications disallow flanges with $b_f / t_f > 24$ to ensure efficient use of the material and to facilitate fabrication and construction.

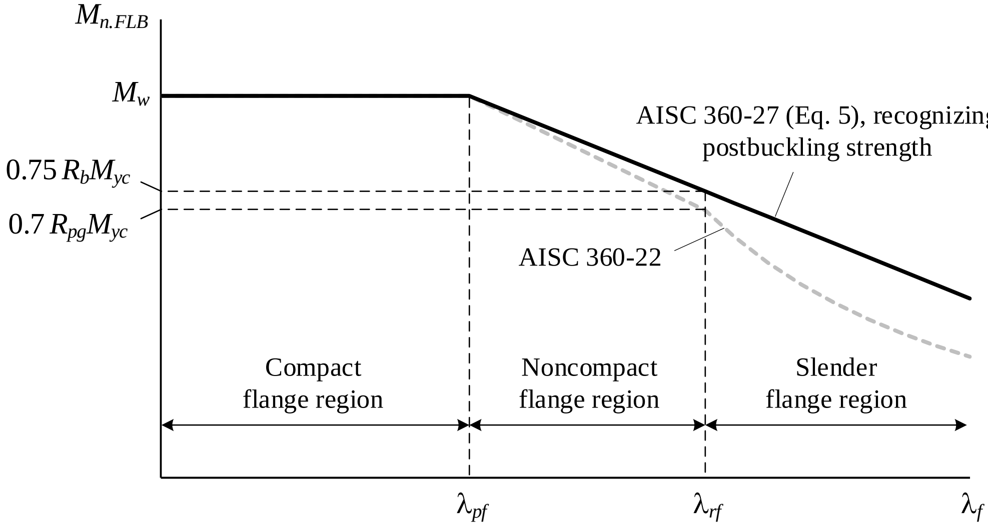

Figure 3: FLB resistance as a function of the flange slenderness λ_f

The FLB strength is addressed separately and independently from LTB in the proposed AISC 360 Chapter F provisions, similar to the approach in the prior AISC 360 rules. Prior experimental test results have demonstrated the lack of any interaction between the FLB and LTB strengths in I-section members for λ_f values employed in ordinary practice (White 2008; White and Jung 2008).

2.3 Lateral-torsional buckling (LTB)

The draft AISC 360-27 Section F3 defines the LTB resistance using the following three equations as illustrated in Fig. 4:

(a) When $\lambda_{LT} \leq \lambda_{pLT}$, the LTB resistance is given by the "plateau" strength

$$M_n = M_w \tag{6a}$$

(b) When $\lambda_{pLT} < \lambda_{LT} \leq \lambda_{rLT}$, the LTB resistance is defined by the inelastic LTB equation

$$M_n = M_w - \left(M_w - R_b M_L\right)\left(\frac{\lambda_{LT} - \lambda_{pLT}}{\lambda_{rLT} - \lambda_{pLT}}\right) \leq R_b F_{cr} S_{xc} \tag{6b}$$

and (c) When $\lambda_{LT} > \lambda_{rw}$, the LTB resistance is defined by the elastic LTB equation

$$M_n = R_b F_{cr} S_{xc} \tag{6c}$$

where

$$\lambda_{LT} = \sqrt{\frac{F_y}{F_{cr}}} \tag{7}$$

is the nondimensional LTB slenderness, M_L is the moment level at the onset of significant inelastic LTB effects, taken as

$$M_L = 0.5 M_{yc} \tag{8}$$

for built-up I-section members and

$$M_L = 0.7 M_{yc} \tag{9}$$

for rolled I-section members, and F_{cr} is the elastic critical moment for LTB.

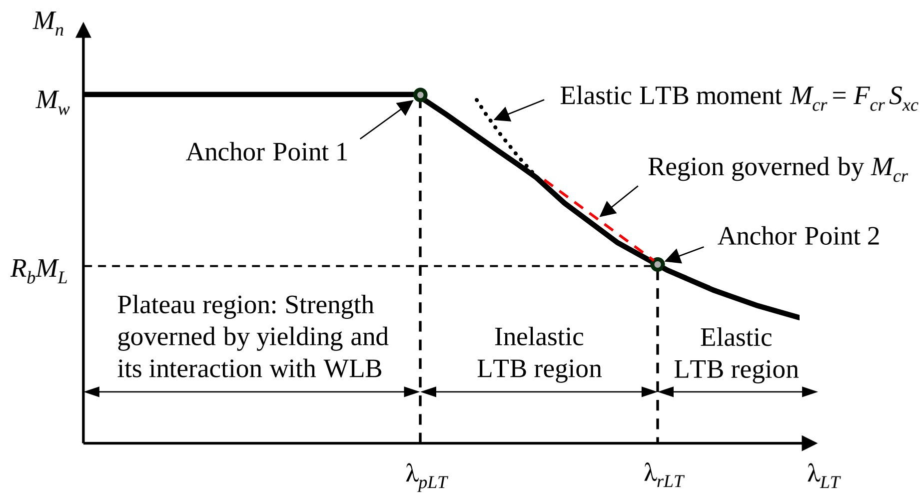

Figure 4: LTB resistance as a function of LTB slenderness λ_{LT}

The use of the nondimensional LTB slenderness λ_{LT} allows for the streamlined quantification of the LTB resistance by Eqs. 6. Furthermore, λ_{LT} is fundamental to the characterization of the LTB resistance as elastic, inelastic, or plastic buckling. For large λ_{LT}, the LTB limit state is elastic and the strength can be written directly in terms of the elastic buckling resistance, whereas for smaller λ_{LT}, it is characterized as inelastic or plastic leading to more significant reductions in the strength relative to the theoretical elastic LTB resistance.

Anchor Points 1 and 2 of the LTB Strength Curve

As shown in Fig. 4, the inelastic LTB Eq. 6b is simply a linear transition between two anchor points, Anchor Point 1 (λ_{pLT}, M_w) and Anchor Point 2 ((λ_{rLT}, $R_b M_L$). Anchor Point 2 is the simpler of the two anchor points in characterizing the strengths. At Anchor Point 2, the elastic LTB resistance before applying the R_b factor, $M_{cr} = F_{cr} S_{xc}$, is equal to M_L. Therefore, the abscissa for Anchor Point 2 is

$$\lambda_{rLT} = \sqrt{\frac{F_y}{M_L / S_{xc}}} \tag{10}$$

For doubly-symmetric sections and singly-symmetric sections with $S_{xt} > S_{xc}$, Eq. 10 gives $\lambda_{rLT} = 1.41$ for $M_L = 0.5M_{yc}$ and 1.20 for $M_L = 0.7M_{yc}$. For sections with $S_{xt} < S_{xc}$, λ_{rLT} is greater than 1.41 since $M_L = 0.5M_{yc}$ and M_{yc}, defined at first yielding of the compression flange, is greater than $F_{yc} S_{xc}$.

Engineers often interpret that $M_L = 0.5M_{yc}$ or $0.7M_{yc}$ implies an initial flange compressive residual stress of $0.5F_{yc}$ or $0.3F_{yc}$. However, the onset of yielding and its effect on the LTB resistance is influenced significantly by amplified compression flange lateral bending as the elastic LTB strength limit state is approached in the vicinity of $\lambda_{LT} = \lambda_{rLT}$. The physical beam or girder is not just in major-axis bending as typically idealized for design.

The abscissa for Anchor Point 1, which may be referred to as the plateau length, is a function of the web slenderness:

(a) When $\lambda_w \leq 0.7\,\lambda_{pw}$

$$\lambda_{pLT} = \lambda_{pLT}' \tag{11a}$$

(b) When $0.7\lambda_{pw} < \lambda_w \leq \lambda_{rw}$

$$\lambda_{pLT} = \lambda_{pLT}' - \left(\lambda_{pLT}' - 0.35\right)\left(\frac{\lambda_w - 0.7\lambda_{pw}}{\lambda_{rw} - 0.7\lambda_{pw}}\right) \tag{11b}$$

and (c) When $\lambda_w > \lambda_{rw}$

$$\lambda_{pLT} = 0.35 \tag{11c}$$

where

$$\lambda_{pLT}' = \frac{1}{\sqrt{C_b}}\left(0.35 + \frac{\left(1 - 1/C_b\right)\left(\lambda_{rLT} - 0.35\right)}{\left(1 - R_b M_L / M_w\right)}\right) \leq 0.8 \tag{12}$$

Equations 7 and 11c recognize that for slender-web members (i.e., for $\lambda_w > \lambda_{rw}$), the mapping from the theoretical elastic LTB strength to the inelastic LTB resistance is relatively simple. The plateau resistance is reached when $\lambda_{LT} = \lambda_{pLT} = 0.35$, independent of moment gradient (i.e., for any value of the moment gradient modifier, C_b). The value $\lambda_{pLT} = 0.35$ corresponds to a ratio of the elastic LTB stress to the yield strength of $F_{cr} / F_y = (1/0.35)^2 = 8.16$. This ratio is the same as the F_{cr} / F_y specified for Anchor Point 1 in the AISC/MBMA Design Guide 25 (White et al. 2021). For uniform bending, $\lambda_{pLT} = 0.35$ and $F_{cr} / F_y = 8.16$ also correspond to the equation for L_p in Sections F4 and F5 of the AISC 360-22 Specification.

For moment gradient, i.e., $C_b > 1.0$, the inelastic LTB strength increases due to the decrease in λ_{LT} with increasing F_{cr}. However, the increase in strength is relatively minor compared to the aggressive rise in the LTB resistance with increasing C_b postulated by the traditional application of C_b in the AISC 360 Specification.

Recent experimental and analytical studies (Phillips et al. 2023a and b, 2024a and b; Deshpande et al. 2024) have demonstrated the accuracy of the above approach for slender-web members. However, the research shows that the Design Guide 25 approach tends to give a conservative representation of the plateau length for stocky-web members subjected to moment gradient. For members with $\lambda_w \leq 0.7\lambda_{pw}$, the traditional application of C_b employed in AISC 360-22 Specification provides an accurate representation of the increased LTB resistance up to a maximum value of $\lambda_{pLT} = 0.8$ (Phillips et al. 2024b).

Figure 5 illustrates the effect of increasing λ_{pLT} from 0.35 for uniform bending to a larger value for moment-gradient cases in members with noncompact- or compact-webs. For larger values of C_b, the linear transition between Anchor Point 2 (λ_{rLT}, M_L) and Anchor Point 1 (λ_{pLT}, M_w) can give values greater than the elastic LTB resistance. Therefore, in Eq. 6b, the LTB resistance is taken as the smaller of the values from the linear interpolation between the anchor points and the elastic LTB resistance. In essence, this increases the moment level corresponding to the onset of significant yielding effects in certain instances.

Figure 5 also illustrates the impact of the FLB resistance calculation for members with noncompact or slender flanges in the context of the LTB strength curve. In the new and prior AISC 360 provisions, the FLB resistance is an independent calculation that works effectively as a cut-off on the LTB strength.

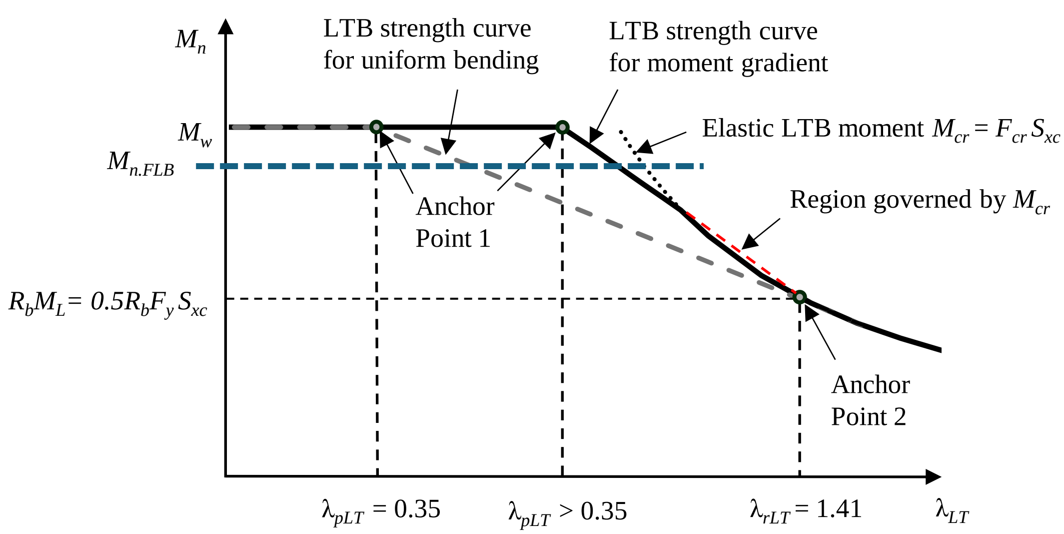

Figure 5: Effect of increasing λ_{pLT} from 0.35 for uniform bending to a larger value for moment-gradient cases in built-up I-section members with noncompact or compact webs

Figure 6 illustrates the impact of C_b on the LTB strength in the traditional AISC 360 Specification approach, shown in terms of the effective unbraced length KL_b and using the new Section F3 parameters M_w and R_b. The base LTB resistance for uniform bending ($C_b = 1.0$) is represented by the dashed grey curve. In the traditional AISC 360 approach, the C_b factor, which is derived as the ratio of the elastic LTB resistance considering the moment gradient to the elastic LTB resistance for uniform bending, is applied as a multiplier on the entire LTB strength curve, irrespective of whether the resulting level of the moment might result in significant strength reductions due to yielding effects. The traditional AISC provisions limit the increase in strength due to C_b only by capping the maximum resistance by M_w. As such, the traditional approach results in anomalous situations in which the design resistance may be taken as the theoretical elastic LTB strength all the way up to $M_w = M_p$ for compact-web members as shown in Fig. 5. Eetikala et al. (2025) show that the above AISC 360 idealization tends to over-estimate the available experimental results for cases where the resulting modified plateau length approaches L_r even for rolled I-section members. Phillips et al. (2023a and b, 2024b) show substantial overprediction by the traditional AISC 360 approach for slender-web members.

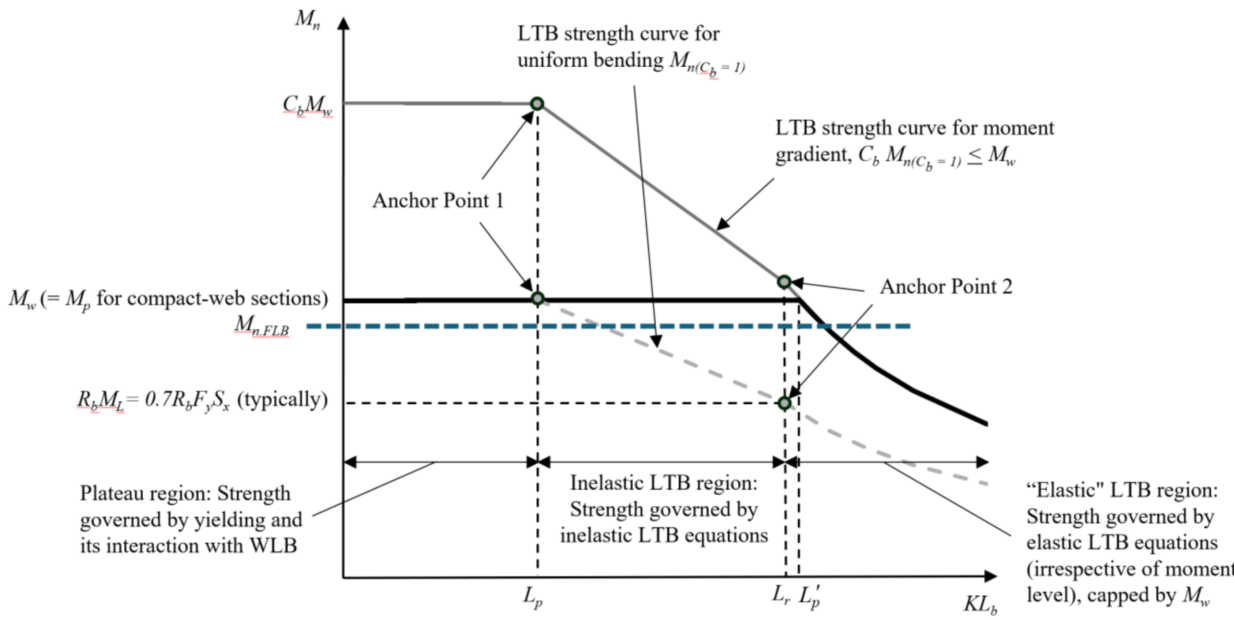

Figure 6: Traditional application of C_b in AISC 360.

For cases where the resulting plateau length, shown as L_p' in Fig. 6, is less than or equal to L_r, the plateau length may be written algebraically as

$$L_p{}' = L_p + \frac{(1-1/C_b)(L_r - L_p)}{(1-R_bM_L/M_w)} \tag{13}$$

Equation 12 is the same as Eq. 13 but is written in terms of the nondimensional slenderness λ_{LT} and it has a maximum limit on the corresponding nondimensional plateau length of 0.8. A simpler approximate expression is proposed for λ_{pLT}' in the current Ballot 2 draft of the new Section F3. Equation 12 is recommended since it matches the behavior of the traditional AISC equations for members with $\lambda_w \leq 0.7\lambda_{pw}$. Equation 11b is a linear interpolation between Eqs. 11a (equal to Eq. 12) and 11c for members with intermediate web slenderness.

In the new Section F3 provisions, the web bend buckling strength reduction factor is applied to the entire LTB strength curve to approximate both the effects of loss of effectiveness of the slender web due to local bend buckling under flexural compression at the plateau strength (which is the case from which the equation for R_b is derived), and the effects of lateral distortion of the cross-section on the inelastic and elastic LTB resistances for the base uniform moment case, irrespective of the moment gradient or the web shear (see Eqs. 1c, 5, 6b, and 6c). For noncompact or compact webs, $R_b = 1.0$.

Impact of Web Shear on the Elastic LTB Resistance

In addition to the above improvements, the proposed Section F3 provisions recognize a significant impact of the web shear force on the elastic LTB resistance for slender- and noncompact-web I-section members (Liang et al. 2021 and 2024). The AISC 360-22 Specification Section F5 uses J = 0 for slender-web I-section members to calculate the elastic LTB resistance. Liang et al. show this idealization can result in substantial conservatism in some cases while not sufficiently accounting for the cross-section distortion and strength reduction caused by the web shear in other cases.

For slender-web members, the impact of shear on the elastic LTB resistance is addressed by applying a reduction factor

$$C_{mv} = C_{mvs} = \frac{V_{cr}}{V_{cr} + \alpha V_{st}} \geq \frac{1}{1+\alpha} \tag{14}$$

along with C_b in calculating the elastic LTB resistance, where V_{cr} is the elastic shear buckling strength of the web, V_{st} is the average web shear within the unbraced length under consideration at the elastic LTB moment obtained from thin-walled open-section beam theory, i.e., not considering any web distortion effects), but not greater than the web shear associated with the moment level $R_b M_L$:

$$V_{st} = \gamma_{cr.st} V_{avg} \leq \frac{R_b M_L}{M_{max}} V_{avg} \tag{15}$$

where $\gamma_{cr.st}$ is the ratio of the elastic LTB moment to the factored moment from thin-walled open-section beam theory (not considering web distortion effects), V_{avg} is the average shear within the unbraced length for the factored loading condition being evaluated, and M_{max} is the maximum moment within the unbraced length under consideration for the factored loading condition.

The subscript "*st*" in V_{st} and $\gamma_{cr.st}$ emphasizes that the thin-walled open-section beam theory solution corresponds to a web that is fully "stiffened" such that any cross-section distortions due to shear effects are prevented.

The last term in Eq. 15 is recommended as a limit to avoid an over-conservative application of C_{mvs} within the inelastic LTB range.

The elastic buckling load ratio may be calculated as

$$\gamma_{cr.st} = \frac{M_{cr.st}}{M_{\max}} \tag{16}$$

where $M_{cr.st}$ can be determined from the equation

$$M_{cr.st} = \frac{C_b \pi^2 E}{\left(\frac{KL_b}{r_T}\right)^2} S_{xc} \sqrt{1 + 0.078 \frac{J}{S_{xc} h_o} \left(\frac{KL_b}{r_T}\right)^2} \tag{17}$$

for prismatic unbraced lengths or by an elastic buckling analysis based on thin-walled open-section beam theory. In Eq. 17, KL_b is the effective unbraced length for LTB, r_T is the radius of gyration of the compression flange plus one-third of the depth of the web in flexural compression, J is the St. Venant torsion constant, and h_o is the distance between the mid-thickness of the flanges.

Lastly, the term α in Eq. 14 is defined as

$$\alpha = 0.11 C_b \sqrt{A_w / A_{fc}} \tag{18}$$

where $A_w = dt_w$, $A_{fc} = b_{fc}\, t_{fc}$, and d is the total cross-section depth. By inspecting the combined Eqs. 14 and 18, one can observe that the largest reductions in the elastic LTB resistance due to web shear occur in unbraced lengths with large C_b, large A_w / A_{fc}, and large V_{st} / V_{cr}.

Given the C_{mv} factor, the elastic LTB stress in Eq. 7 is calculated as

$$F_{cr} = C_{mv} M_{cr.st} / S_{xc} \tag{19}$$

It should be noted that it is always conservative to design using the uniform bending LTB strength with $C_b = 1.0$, in which case C_{mv} is also equal to 1.0. In addition, it is recommended that C_{mv} be taken equal to 1.0 in all situations where $C_b \leq 1.4$ to simplify the design calculations, avoiding situations where the engineer would perform the additional calculations only to find that the final M_n from Eqs. 6 is practically unaffected. Also, for noncompact-web members, the Section F3 provisions define a linear interpolation between $C_{mv} = C_{mvs}$ at the noncompact-web limit and $C_{mv} = 1.0$ at the compact-web limit, discounting any theoretical strength reduction from C_{mvs} in the limit that the web is compact.

2.4 Representative Results – Three-Point Bending Tests

Figure 7 compares the predictions by the AISC 360-22 Section F5, the new AISC Section F3, and the second-generation Eurocode 3 (CEN 2022) provisions, Section 8.3.2.3(3), to the results from FEA test simulation for a representative suite of welded I-section members studied experimentally and analytically by Phillips et al. (2023a and b; 2024b). The members in this demonstration are doubly symmetric with nominal 6 in. x 3/8 in. flanges and 36 in. x 5/16 in. webs. The members were loaded in three-point bending, they had torsionally and flexurally simply-supported end conditions (i.e., fork end conditions), and they were braced at the mid-span load point. The simulations were conducted using an expected yield strength of $F_y = 60$ ksi for the design of the experimental testing. Experimental testing confirmed the substantial overprediction of the LTB resistance by the AISC 360-22 provisions and the accuracy of the new AISC 360 Section F3 approach (Phillips et al. 2023a). The recommended Section F3 provisions and the second-generation Eurocode 3 provisions successfully capture the test simulation results with some degree of conservatism. The reader is referred to Phillips et al. (2023a and b; 2024b) for detailed discussions of the results.

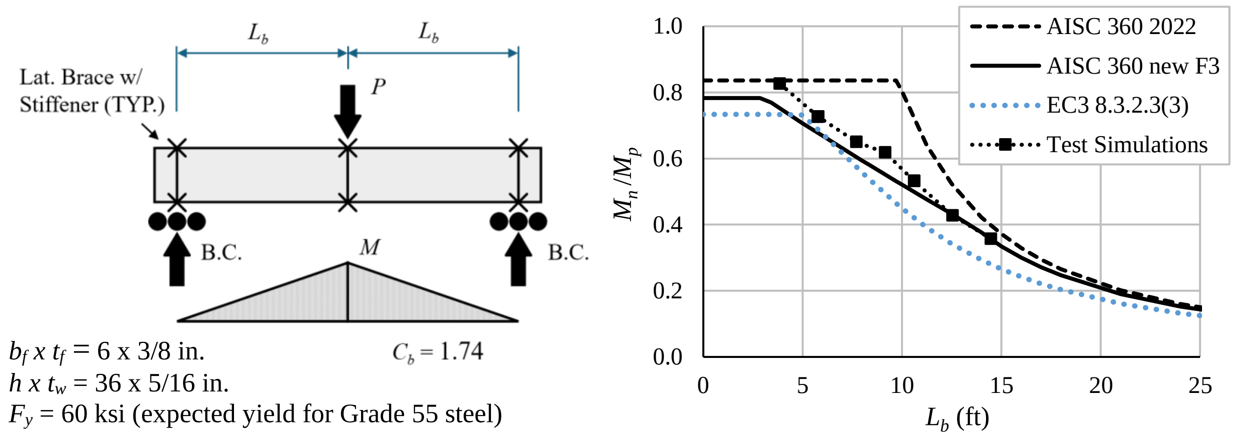

Figure 7: Comparison of AISC 360-22, new AISC Section F3, and second-generation Eurocode 3 predictions to FEA test simulation results for representative welded I-section members in three-point bending

2.5 Nonprismatic member design

The new AISC 360 Section F3 provisions easily accommodate the design of nonprismatic I-section members for flexural loading. For nonprismatic members, the AISC 360 provisions may be applied to check the LTB resistance by utilizing an essential concept introduced in the AISC/MBMA Design Guide 25 (White et al. 2021) and illustrated by Fig. 8.

Given a potentially critical cross-section, the strength verification is conducted by considering a hypothetical "equivalent" prismatic member having the same M_u/M_w and the same $\gamma_{cr.st}$ as the general nonprismatic member. The elastic buckling load ratio, $\gamma_{cr.st}$, may be determined by various hand-calculation procedures as discussed by Design Guide 25; however, $\gamma_{cr.st}$ is also fundamentally the eigenvalue obtained from an elastic buckling analysis considering the member with its actual end or continuity conditions in a larger structure. Software such as ConSteel (2025) can be employed to accurately model a general framing system composed of general nonprismatic members and to calculate $\gamma_{cr.st}$. Given $\gamma_{cr.st}$, the engineer first calculates $F_{cr} = \gamma_{cr.st} f_{bu}$ at the cross-section under consideration, where $f_{bu} = M_u / S_{xc}$. They then determine the member demand-to-capacity ratio (DCR) corresponding to that cross-section, $DCR = M_u/\phi_b M_n$ in LRFD, by performing the AISC 360 calculations for the hypothetical equivalent prismatic member that has the same M_u/M_w and $\gamma_{cr.st}$.

Generally, a nonprismatic member's LTB resistance must be checked by considering several potentially critical cross-sections. The concept is the same as generally needing to check each member in a frame composed of multiple members. The governing member *DCR* is the largest one from the various checks. If all the cross-sections in the unbraced length under consideration have noncompact to compact webs, the LTB resistance is critical at the cross-section where M_u/M_w is the largest. However, if the nonprismatic member has slender-web sections, the behavior of the equations is such that the engineer may need to check several slender-web cross-sections with large M_u/M_w. If one applies the smallest R_b of all the cross-sections under consideration in the calculation of M_w for all the cross-sections, then the cross-section with the largest M_u/M_w is ensured to govern.

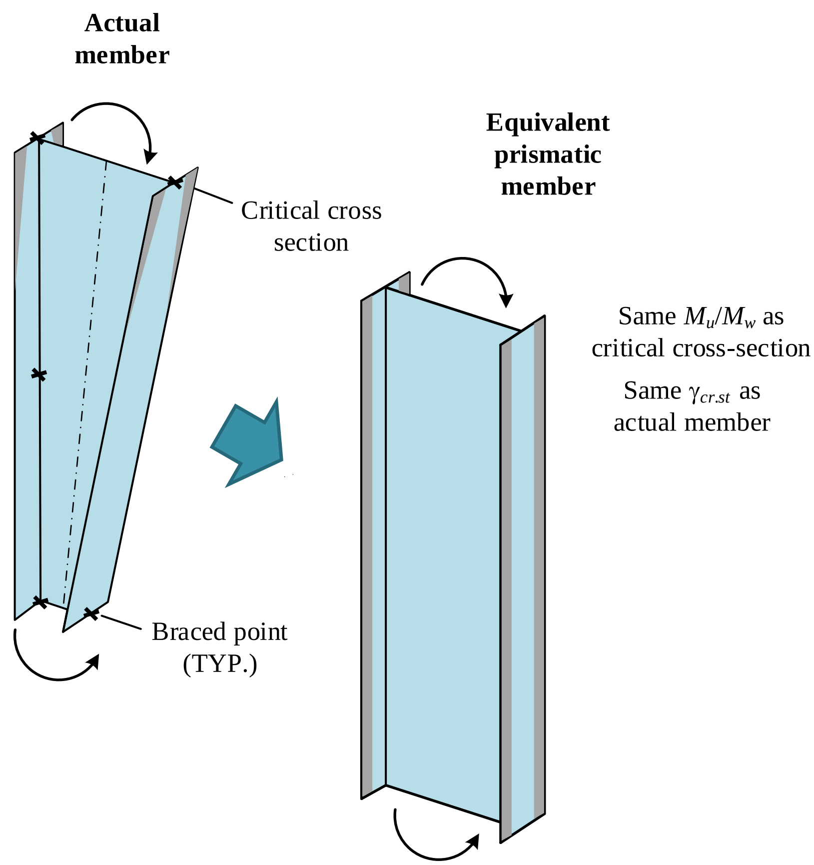

Figure 8: Concept of an equivalent prismatic member having the same M_u/M_w as the potentially critical cross-section and the same elastic buckling eigenvalue $\gamma_{cr.st}$

Nonprismatic members generally require the calculation of a different C_b than prismatic members. Design Guide 25 provides guidance. The alternative calculation of C_b is necessary since the compression flange stresses vary along the unbraced length as a function of the nonprismatic geometry. Applying prismatic member Cb equations to nonprismatic members can yield significantly unconservative results. Fortunately, in many situations involving nonprismatic members, C_b is less than 1.4; therefore, C_{mv} may be taken equal to 1.0 without any significant impact on the results.

The reader is reminded that the FLB check is a separate and independent strength evaluation. For nonprismatic members, the FLB evaluation amounts to cross-section-by-cross-section checks.

3. Combined Axial Compression and Flexure

The General Method is recommended to address the strength verification for cases involving combined axial loading and flexure. Vaszilievits-Sömjén et al. (2023) provide a detailed discussion of the method in the context of the AISC 360 Specification. The following is a brief outline of the steps:

(a) Perform an in-plane geometric nonlinear analysis to determine the force demands. In the context of the AISC 360 Specification, the Direct Analysis Method rules are recommended for these calculations, thereby addressing the global in-plane structural stability considerations.

(b) Determine the member demand-to-capacity ratios (DCR) for the various potentially critical cross-sections. Per AISC 360

$$DCR = \frac{P_u}{\phi_c P_n} + \frac{8}{9}\frac{M_{ux}}{\phi_b M_{nx}} \quad \text{for } \frac{P_u}{\phi_c P_n} \geq 0.2 \tag{20a}$$

$$DCR = \frac{P_u}{2\phi_c P_n} + \frac{M_{ux}}{\phi_b M_{nx}} \quad \text{for } \frac{P_u}{\phi_c P_n} < 0.2 \tag{20b}$$

where P_u is the cross-section axial force demand, and $\phi_c P_n$ is the axial compressive resistance, which is calculated for a nonprismatic member in a manner similar to that discussed in Section 2.5 for determining $M_{ux}/\phi_b M_{nx}$. That is, given the cross-section strength ratio P_u/P_{ye} and the member elastic buckling load ratio γ_{cr}, one calculates the $\phi_c P_n$ of an equivalent prismatic member having the same P_u/P_{ye} and γ_{cr}. In this calculation, P_{ye} is the yield load for the effective cross-section used in determining the axial compressive resistance, $P_{ye} = F_y A_e$, where A_e is the effective cross-sectional area. The AISC 360 column strength formula is defined explicitly in terms of $\lambda^2 = P_y/P_{cr} = F_y/F_{cr}$, where P_y is the yield load on the gross cross-sectional area, $P_y = F_y A_g$, and $P_{cr} = \gamma_{cr} P_u$ at the cross-section under consideration, which facilitates the calculations. Design Guide 25 provides guidance for the hand calculation of γ_{cr}; however, modern software systems can be employed to determine γ_{cr} in a more automated and rigorous manner. The ratio $M_{ux}/\phi_b M_{nx}$ is calculated as discussed in Section 2. (It is implied throughout these discussions that the in-plane bending is about the cross-section's major axis, and the LTB limit state involves twisting and out-of-plane bending about the cross-section's minor axis.)

AASHTO LRFD (AASHTO 2024) recommends a more conservative *DCR* calculation for members containing any slender cross-section elements:

$$DCR = \frac{P_u}{\phi_c P_n} + \frac{M_{ux}}{\phi_b M_{nx}} \tag{20c}$$

(c) The General Method simplifies and streamlines the elastic buckling analysis and the strength evaluation by directly determining the out-of-plane member elastic buckling load ratio $\gamma_{cr.op}$ from a computational model of the structure. This ratio is combined with the gross cross-section demand-to-capacity ratio at a potentially critical cross-section,

$$DCR_{cs} = \frac{P_u}{P_y} + \frac{M_{ux}}{M_{ycx}} \tag{21}$$

to calculate the member's out-of-plane nondimensional slenderness

$$\lambda_{op} = \sqrt{\frac{1}{\gamma_{cr.op}\ DCR_{cs}}} \tag{22}$$

The member’s λ_{op} is then employed for λ in the column axial capacity equations and λ_{LT} in the LTB resistance Eqs. 6 to determine the $\phi_c P_n$ and $\phi_b M_{nx}$ values. These capacities are then substituted with the demands P_u and M_{ux} into the appropriate Eq. 20 to determine the member *DCR* values.

It should be noted that the FLB flexural resistance also needs to be addressed in the above calculations. The FLB flexural resistance is considered as a cap on $\phi_b M_n$ when performing the *DCR* calculation in Eqs. 20.

In addition, it should be noted that for members subjected to significant major-axis bending shear in combination with axial loading, the axial compressive resistance should be reduced to account for its interaction with shear. AASHTO LRFD Article 6.9.2.2.2 addresses this interaction in a practical, simplified way.

4. Combined Torsion and Flexure

The AASHTO LRFD (AASHTO 2024) Specifications provide the most succinct and straightforward guidance for handling general combinations of torsion and flexure, with or without axial force, in I-section members. Article C6.9.2.2.2 of these Specifications states:

“In I- and H-section members subjected to torsion, the flanges may be subjected to significant additional lateral bending due to the restraint of warping. The additional flange lateral bending may be considered by calculating M_{uy}/M_{ry} considering each of the individual flanges as a separate component, then combining the larger of these M_{uy}/M_{ry} values with the strength ratios in the appropriate strength interaction equations. Alternatively, for I-section members subjected to major- and minor-axis bending plus torsion, the one-third rule provisions of Article 6.10 may be employed to assess these combined effects.”

The term M_{ry} is a shortened notation in AASHTO LRFD for $\phi_b M_{ny}$. The reader is referred to Article 6.10 of the AASHTO LRFD Specification for a discussion of the so-called one-third rule, a useful streamlined characterization of the strength of I-girders subjected to major-axis bending and flange lateral bending. For more general cases, AASHTO LRFD extends Eqs. 20 to the consideration of combined major-axis and minor-axis bending by substituting

$\dfrac{M_{ux}}{\phi_b M_{nx}} + \dfrac{M_{uy}}{\phi_b M_{ny}}$ for each of the occurrences of $\dfrac{M_{ux}}{\phi_b M_{nx}}$ in the equations.

The strength $\phi_b M_{ny}$ in the AISC 360 and AASHTO LRFD Specifications is either a yielding or a flange local buckling calculation. It should be noted that the compact-flange limit for minor-axis bending has been increased in the draft AISC 360-27 Specification to recognize better the limit states behavior in minor-axis bending. When considering the $\phi_b M_{ny}$ based on an individual flange as recommended in the above AASHTO LRFD excerpt, the resistance is calculated based on the individual flange plastic and yield moment $M_{pf} = F_y\, t_f\, b_f^{\,2}/4$ and $M_{yf} = F_y\, t_f\, b_f^{\,2}/6$, respectively. Also, the elastic weak-axis bending moment demand on the entire cross-section should be apportioned to the individual flanges in proportion to their lateral bending moments of inertia, $I_{yf} = t_f\, b_f^{\,3}/12$.

Various approximate calculations are recommended in AASHTO LRFD for the first-order flange lateral bending moment due to warping torsion (see Articles C4.6.1.2.4b and C6.10.3.4.1). Generally, these first-order lateral bending moments are amplified by the second-order effects from the flexural compression from the major-axis bending moment, M_{ux}, plus any axial compression, P_u, supported by the member. AASHTO Article 6.10.1.6 gives simple amplification factors based on idealizing the compression flange as a beam-column subjected to axial compression from the major-axis bending. These equations can be applied to estimate the maximum second-order elastic flange lateral bending moments given the first-order moments. However, these equations only consider the amplification caused by the major-axis bending moments. The engineer can perform similar idealizations of the flange as an equivalent beam-column to incorporate the effect of member axial compression.

More rigorous second-order elastic solutions can be obtained for the flange lateral bending moment M_{uyf} using three-dimensional frame analysis capabilities based on thin-walled open-section beam theory, such as provided by ConSteel (ConSteel 2025). Given the second-order bimoment at a cross-section calculated by the software, the flange lateral bending moment in a general singly-symmetric I-section member may be determined as follows:

$$M_{uyf} = \frac{B a_y I_{yf}}{C_w} \tag{23}$$

where B is the bimoment, a_y is the distance from the cross-section shear center to the mid-thickness of the flange under consideration, $I_{yf} = t_f\, b_f^{\,3}/12$ is the lateral bending moment of inertia of the flange, and

$$C_w = \frac{h_o^2 I_{yf1}}{\dfrac{I_{yf1}}{I_{yf2}} + 1} \tag{24}$$

where I_{yf1} and I_{yf2} are the two flanges' respective lateral bending moments of inertia.

For problems involving flange lateral bending moments, M_{uyf}, in addition to P_u and/or M_{ux}, it should be noted that M_{uyf} commonly has negligible influence on the elastic eigenvalue $\gamma_{cr.op}$. Therefore, $\gamma_{cr.op}$ can be calculated considering just P_u and M_{ux}. However, M_{uyf} can have significant second-order amplification due to the stability effects associated with $\gamma_{cr.op}$.

4. Conclusions

The AISC 360 new Section F3 provisions under consideration during the 2027 Specification development cycle provide an improved, streamlined calculation of the flexural resistance of general I-section members. The calculations address significant attributes related to moment gradient and corresponding web shear that previously have not been understood and addressed. The new AISC 360 provisions may be combined with concepts from the General Method (CEN 2022) plus simplified strength interaction equations for axial force, flexure, shear, and flange lateral bending due to warping torsion to address the wide range of potential loadings encountered in engineering practice.

Acknowledgments

The impactful research studies by the first author's faculty colleague, Dr. Ryan Sherman, and their research team at Georgia Tech – Ajinkya Deshpande, Aakash Reddy Eetikala, Ajit Kamath, Matthew Phillips, Ryan Slein, Lakshmi Subramanian, and Oğuzhan Toğay – are gratefully acknowledged. The impactful research studies by Dr. Todd Helwig, his faculty colleagues, Drs. Michael Engelhart and Joe Yura, and his research team – Chen Liang, Matthew Reichenbach, Zhihua Xiong, and Zhenhua Pen – are also gratefully acknowledged. The substantial efforts by the AISC Technical Committee 4 (TC4) Chairs Lou Geschwindner and Ben Schafer, and by the TC4 members during the AISC 2022 and 2027 Specification cycles, are much appreciated. Research funding by the Metal Building Manufacturers Association, the American Institute of Steel Construction, and the American Iron and Steel Institute was essential in driving the Georgia Tech research. The attention to the AISC Specification research by ConSteel Software Systems, and the development of the Eurocode 3 General Method and its application in the context of the AISC 360 provisions by ConSteel, are gratefully acknowledged. The opinions expressed in the papers are those of the authors and do not imply any endorsement by their colleagues and supporting organizations.

References

AASHTO (2024). *AASHTO LRFD Bridge Design Specifications*, 10th ed., American Association of State Highway and Transportation Officials, Washington, DC.

AASHTO (2020). *AASHTO LRFD Bridge Design Specifications*, 9th ed., American Association of State Highway and Transportation Officials, Washington, DC.

AISC (2022). *Specification for Structural Steel Buildings*, American Institute of Steel Construction Chicago, IL.

CEN (2022). *Eurocode 3 – Design of Steel Structures – Part 1-1: General Rules and Rules for Buildings*, EN 1993-1-1, Comité Européen de Normalisation, Brussels.

ConSteel (2025). consteelsoftware.com, accessed Feb. 21, 2025.

Deshpande, A.M., Sherman, R.J., and White, D.W. (2024). "Influence of transverse stiffening on the lateral-torsional buckling resistance of built-up I-girders," *Thin-Walled Structures*, 195, February, https://doi.org/10.1016/j.tws.2023.111320.

Eetikala, A.R., White, D.W., and Sherman, R.J. (2025). "Comparison of AISC 360 and Eurocode 3 lateral-torsional and flange local buckling predictions to results from a comprehensive experimental database for rolled I-section members," *Proceedings of the Annual Stability Conference*, Structural Stability Research Council, April, to appear.

Latif, W. and White, D.W. (2022). "Flange Local Buckling Resistance and Local-Global Buckling Interaction in Slender Flange Welded I-Section Beams," Engineering Journal, American Institute of Steel Construction, 59(2), 113-134.

Liang, C., Xiong, Z., Helwig, T.A., Reichenbach, M.C., and Pan, Z. (2024). "Effects of shear on the lateral torsional buckling of singly-symmetric I-beams," *Thin-Walled Structures*, 203, https://doi.org/10.1016/j.tws.2024.112174.

Liang, C., Reichenbach, M.C., Helwig, T.A., Engelhardt, M.D., and Yura, J.A. (2021). "Effects of shear on the elastic lateral torsional buckling of doubly symmetric I-beams," *Journal of Structural Engineering*, ASCE, 148(3), https://doi.org/10.1061/(ASCE)ST.1943-541X.0003294.

Phillips, M., Slein, R., Sherman, R.J., and White, D.W. (2024a). "Experimental database for lateral-torsional buckling of built-up I-section members," *Mendeley Data*, V1, doi: 10.17632/v2pr9rbxyk.1.

Phillips, M., Slein, R., Sherman, R.J., and White, D.W. (2024b). "Proposed improvements to AISC 360-22 Chapter F for built-up I-section members," *Journal of Constructional Steel Research*, 217, https://doi.org/10.1016/j.jcsr.2024.108657.

Phillips, M., Slein, R., Sherman, R.J. and White, D.W. (2023a). "Experimental investigation of doubly-symmetric built-up I-girders subjected to high moment gradient)," *Engineering Structures*, 283, May, https://doi.org/10.1016/j.engstruct.2023.115724.

Phillips, M., Kamath, A.M., Sherman, R.J. and White, D.W. (2023b). "Influence of web distortion and onset of yield on doubly symmetric built-up I-girders subjected to high moment gradient," *Thin-Walled Structures*, 185, April, https://doi.org/10.1016/j.tws.2023.110545.

Slein, R., Kamath, A.M., Phillips, M., Toğay, O., Sherman, R.J., and White, D.W. (2024). "Flexural resistance of thin-web singly-symmetric steel I-sections exhibiting early tension flange yielding," *Journal of Constructional Steel Research*, 221, https://doi.org/10.1016/j.jcsr.2024.108831.

Subramanian, L. and White, D.W. (2017). "Improved noncompact web slenderness limit for steel I-girders," *Journal of Structural Engineering*, ASCE, 143(4), https://doi.org/10.1061/(ASCE)ST.1943-541X.0001722.

Vaszilievits-Sömjén, B., Szalai, J. and White, D.W. (2023). "Frame design using nonprismatic members – satisfying the need for speed," *Proceedings of the Annual Stability Conference*, Structural Stability Research Council Charlotte, North Carolina, April 11-14, 2023.

White, D.W., Jeong, W.Y. and Slein, R. (2021). *Design of Frames Using Nonprismatic Members*, AISC/MBMA Design Guide 25, 2nd Edition, American Institute of Steel Construction and Metal Building Manufacturers Association, 405 pp.

White, D.W. (2008). "Unified flexural resistance equations for stability design of steel I-section members – Overview," *Journal of Structural Engineering*, ASCE, 134(9), 1405-1424.

White, D.W. and Jung, S.-K. (2008). "Unified flexural resistance equations for stability design of steel I-section members – uniform bending tests," *Journal of Structural Engineering*, ASCE, 134(9), 1450-1470.